A FRONT TRACKING APPROACH TO A MODEL OF CONTINUOUS SEDIMENTATION IN IDEAL CLARIFIER-THICKENER UNITS

R. BÜRGER, K.H. KARLSEN, C. KLINGENBERG, AND N.H. RISEBRO

ABSTRACT. We study a model of continuous sedimentation. Under idealizing assumptions, the settling of the solid particles under the influence of gravity can be described by the initial value problem for a one-dimensional scalar conservation law with a flux function that depends discontinuously on the spatial position. We construct a weak solution to the sedimentation model by proving convergence of a front tracking method. The basic building block in this method is the solution of the Riemann problem, which is complicated by the fact that the flux function is discontinuous. A feature of the convergence analysis is the difficulty of bounding the total variation of the conserved variable. To overcome this obstacle, we rely on a certain nonlinear Temple functional under which the total variation can be bounded. The total variation bound on the transformed variable also implies that the front tracking construction is well defined. Finally, via some numerical examples, we demonstrate that the front tracking method can be used as a highly efficient and accurate simulation tool for continuous sedimentation.

1. INTRODUCTION

We consider a model of continuous sedimentation of ideal suspensions of small solid particles dispersed in a viscous fluid. Under idealizing assumptions, the settling of the solid particles under the influence of gravity can be described by the one-dimensional kinematic sedimentation theory formulated by Kynch [25]. This theory models the suspension as a mixture of two superimposed continuous media, the solid and the fluid. Its essential assumption states that if v_{s} and v_{f} denote the solid and fluid phase velocity, then the relative velocity of the solids with respect to the fluid, $v_r = v_{\mathrm{s}} - v_{\mathrm{f}}$, is a function of the local solids concentration u only, $v_r = v_r(u)$. This assumption is well justified for suspensions of small rigid spheres showing no floc structure or compressibility effects. A thorough discussion of Kynch's and related sedimentation models is provided in [6].

The basic balance equations are the continuity equations of the solid and of the fluid,

$$u_t + (uv_{\mathrm{s}})_x = 0, \tag{1.1}$$

$$u_t - \big((1-u)v_{\mathrm{f}}\big)_x = 0, \tag{1.2}$$

where t is time and the vertical coordinate x is assumed in this paper to increase downwards. In terms of the volume-average velocity of the mixture $q = uv_{\mathrm{s}} + (1-u)v_{\mathrm{f}}$, the continuity equation of the mixture, obtained as the difference of (1.1) and (1.2), can be written as $q_x = 0$, i.e., $q(\cdot,t)$ is a constant function for each t and is determined by boundary and feed conditions. In particular, $q \equiv 0$ in a closed settling column without in- or outlets.

In terms of the velocities $v_{\mathrm{r}}(u)$ and $q = q(x,t)$, Eq. (1.1) can be rewritten as

$$u_t + \big(q(x,t)u + u(1-u)v_{\mathrm{r}}(u)\big)_x = 0.$$

Date: June 11, 2001.

Key words and phrases. continuous sedimentation, conservation law, discontinuous flux, weak solution, front tracking, convergence, numerical example.

This work was done while Karlsen was visiting the Department of Mathematics and the Institute for Pure and Applied Mathematics (IPAM) at the University of California, Los Angeles (UCLA). K.H. Karlsen is grateful to IPAM for their hospitality and financial support. Furthermore, K.H. Karlsen, C. Klingenberg, and N.H. Risebro thank the project *Nonlinear partial differential equations of evolution type - theory and numerics*, which is part of the BeMatA program of The Research Council of Norway, for financial support.

It is customary to introduce the so-called Kynch batch flux density function $h(u) = u(1-u)v_r(u)$, so that the governing equation takes the form

$$u_t + \big(q(x,t)u + h(u)\big)_x = 0. \tag{1.3}$$

The function h reflects the material dependency of the suspension. The basic assumptions on h can be stated as

$$\operatorname{supp}(h) = [0,1], \quad h(u) > 0 \quad \text{for} \quad u \in (0,1), \quad h'(0) > 0 \quad \text{and} \quad h'(1) \le 0.$$

We have chosen the value "1" as the maximum solids concentration. Since it is not the purpose of this paper to discuss the widest class of model functions, we simply assume h to be sufficiently smooth. The vast majority of Kynch batch flux density functions h determined from settling experiments in the literature have at least one inflection point, see [4, 6].

A very simple model for continuous sedimentation was studied by Bustos et al. [7], in which Eq. (1.3) is restricted to a space interval, say $x \in [0,1]$, corresponding to a cylindrical vessel, and where the upper end $x = 0$ is identified with a feed inlet and the lower $x = 1$ with a discharge outlet. The vessel is assumed to be fed continuously with feed suspension at the inlet (surface source) and to be discharged continuously through the outlet (surface sink). The overflow of clear liquid is not explicitly modelled. The volume average velocity is a function of time only, $q(t) = q_r(t)$, where q_r is a prescribed control function determined by the discharge opening. In the model by Bustos et al. [7], Eq. (1.3) is provided with Dirichlet boundary conditions at $x = 0$ and $x = 1$ and appropriately studied in the framework of entropy boundary conditions [8].

This model, which was proposed first by Petty [27], has some severe shortcomings. Among them is the lack of a global conservation principle due to the use of Dirichlet boundary conditions. It is preferable to replace the boundary conditions at the ends of the vessel by transitions between the transport flux $q(x,t)u$ and the composite flux $q(x,t)u + h(u)$, such that the problem is reduced to a pure initial value problem. Moreover, in a realistic model the feed suspension should enter at a feed level located between the overflow outlet at the top and the discharge outlet at the bottom. This gives rise to an upwards-directed volume average velocity $q_l \le 0$ above and a downwards-directed velocity $q_r \ge 0$ below the feed level. The feed source itself is modeled by a singular source term. Such configurations were proposed by several authors [1, 9, 10, 26] under different names such as clarifier-thickener units or high-capacity thickeners. Particularly thorough analysis of clarifier-thickener models were presented by Diehl in a series of papers [12, 13, 14, 15].

It is such an improved model which is considered in this paper, and its main purpose is to show that front tracking can be employed both as a means to show existence of weak solutions as well as an efficient computational tool to compute approximate solutions of the clarifier-thickener system. To put this observation in the proper perspective, we recall that the main idea behind front tracking was introduced by Dafermos [11]. To illustrate it, consider the conservation law

$$u_t + h(u)_x = 0, \quad x \in \mathbb{R},\ t > 0; \qquad u(x,0) = u_0(x), \quad x \in \mathbb{R}, \tag{1.4}$$

where u_0 is assumed to be piecewise constant. Then the entropy solution can be constructed by a superposition of solutions of Riemann problems, i.e., solutions of the conservation law with initial data consisting of two constant states separated by a simple discontinuity. If the flux h is piecewise linear, each Riemann solution consists exclusively of constant states separated by shocks. When waves from neighboring Riemann problems interact, the interaction will only involve constant states and therefore lead to new Riemann problems and the construction can be continued forward in time. Thus, the construction consists of solving Riemann problems and tracking straight-line discontinuities. In the general case, the initial function is approximated by a step function and the flux by a piecewise linear function. This way rarefaction waves are approximated by a sequence of small shocks. Variants of the method have been used by many authors, see Holden and Risebro [20] for the history and many references. In particular, Holden, Holden, and Høegh–Krohn [19] proved that the construction is well-defined and terminate in a finite number of steps, even for non-convex flux functions, given a finite number of constant states in $u_0(x)$. Front tracking was later formulated for hyperbolic systems by DiPerna[16], Bressan [2] and Risebro [28], who used the method to give an alternative proof of Glimm's famous existence result for hyperbolic systems.

Very recently a modification of the front tracking method was used by Bressan, Liu, and Yang [3] to prove that the limit of the front tracking sequence defines a continuous semigroup. The front tracking method has also turned out to be a successful computational tool for systems of conservation laws. For example, Risebro and Tveito [29, 30] used it to numerically solve the Euler equations of gas dynamics and a non-strictly hyperbolic system modeling polymer flow, see [20] for further references.

Variants of the front tracking technique based on Dafermos' [11] have also been used earlier to compute approximate solution to problems corresponding to batch sedimentation in a column have been presented by Bustos and Concha [5] and Kunik [23, 24]. However, to apply front tracking to the advanced clarifier-thickener model with continuous flow, one must be able to solve Riemann problems that are nonstandard in that changes between flux functions, depending on the space coordinate x, are involved. Such solutions were constructed by Gimse and Risebro [17, 18]. In [17] it was shown that under some mild conditions, Riemann problems with a discontinuous flux functions always had weak solutions. Furthermore, one can always single out a unique weak solution being the limit of a viscous approximation. The paper [18] considered the Cauchy problem for a conservation law modeling two-phase flow in porous media, where the flux function depends discontinuously on the spatial location.

It is the purpose of the present paper to demonstrate that under slight modifications, the techniques advanced in [17, 18] also handle the non-standard Riemann problems occurring in the present application.

The remainder of this paper is organized as follows: In Section 2 the mathematical model is outlined. This model leads to three non-standard Riemann problems, whose solutions are constructed in Section 3. These solutions are then used as a tool in the front tracking algorithm used to determine global weak solutions. In Section 4, we first formulate the front tracking method for the clarifier-thickener problem. Then we show that the variation of a particular nonlinear functional of the approximate solution constructed by front tracking, the so-called Temple functional, is bounded. This result implies that the front tracking construction is well defined, in the sense that there exist only a finite number of interactions between waves for $t > 0$. Finally it is shown that one can let the discretization parameter of the front tracking algorithm tend to zero, which permits to conclude that a weak solution to the settler-clarifier problem exists, and that this weak solution is a limit of a sequence constructed by front tracking. While we are in Section 4 mainly interested in proving existence of a weak solution, we demonstrate in Section 5 by three numerical examples that front tracking provides moreover an efficient numerical tool for the actual computation of weak solutions for practical problems.

2. The mathematical model

Consider the configuration of Figure 1, where $x = -1$, 0 and 1 are assumed to be the levels at which in normal operation, the clarified liquid leaves the equipment (overflow level), the feed suspension in pumped into the unit (feed level), and through which the concentrated sediment leaves the thickener (discharge level), respectively. At $x = 0$, the vessel is fed with fresh suspension at a volume flow rate $Q_{\mathrm{F}}(t) \geq 0$. The volume flow rate of the discharge, $Q_r(t) \geq 0$ or equivalently $q_r(t) = Q_r(t)/S$, where S denotes the constant cross-sectional area of the vessel, is also prescribed. The volumetric balance of the mixture requires that

$$Q_r(t) = Q_l(t) + Q_{\mathrm{F}}(t). \tag{2.1}$$

We assume that the volume flows satisfy $Q_{\mathrm{F}}(t) \geq 0$, $Q_r(t) \geq 0$ and $Q_l(t) \leq 0$. Dividing (2.1) by S shows that

$$q(x,t) = \begin{cases} q_l(t) = q_r(t) - Q_{\mathrm{F}}(t)/S \leq 0 & \text{for } x < 0, \\ q_r(t) \geq 0 & \text{for } x > 0. \end{cases} \tag{2.2}$$

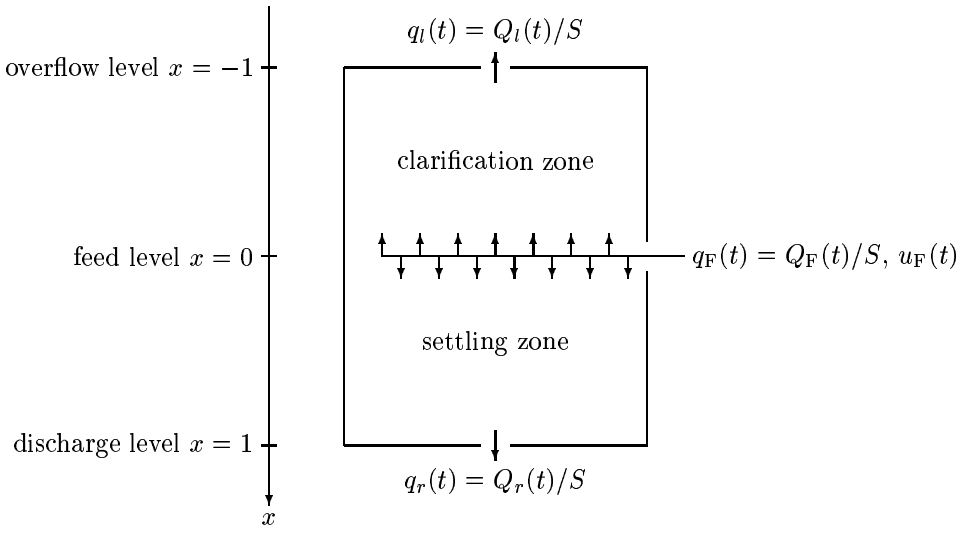

FIGURE 1. The one-dimensional clarifier-thickener model.

The prescribed local volumetric solids concentration of the feed flux is $u_F(t)$. Consequently, the solids continuity equation for $-1 < x < 1$ can be written as

$$u_t + \big(q(x,t)u + h(u)\big)_x = \delta(x)\frac{Q_F(t)u_F(t)}{S}, \tag{2.3}$$

where δ denotes Dirac unit mass located at $x = 0$, and $q(x,t)$ is given by (2.2). Expressing δ as the derivative of the Heaviside function H and noting that

$$q(x,t) = q_l(t) + H(x)(q_r(t) - q_l(t)) = q_l(t) + H(x)\frac{Q_F(t)}{S},$$

we can rewrite (2.3) as

$$u_t + \big(q(x,t)\big(u - u_F(t)\big) + q_l(t)u_F(t) + h(u)\big)_x = 0.$$

Taking into account that the Kynch batch flux density function h is zero outside the interval $(-1,1)$, we finally obtain the conservation law

$$u_t + g(x,t,u)_x = 0, \quad x \in \mathbb{R}, \quad t > 0 \tag{2.4}$$

with the composite flux density function

$$g(x,t,u) = \begin{cases} q_l(t)u & \text{for } x < -1, \\ q_l(t)u + h(u) & \text{for } -1 < x < 0, \\ q_r(t)u + h(u) + \big(q_l(t) - q_r(t)\big)u_F(t) & \text{for } 0 < x < 1, \\ q_r(t)u + \big(q_l(t) - q_r(t)\big)u_F(t) & \text{for } x > 1. \end{cases} \tag{2.5}$$

For the remainder of this paper we regard $q_l(t)$, $q_r(t)$ and $u_F(t)$ as independent control variables satisfying $q_l(t) \le 0$, $q_r(t) \ge 0$ (then we always have $Q_F(t) = S(q_r(t) - q_l(t)) \ge 0$) and $0 \le u_F(t) \le 1$. We shall also also assume that the control variables q_l, q_r and $0 \le u_F \le 1$ are constant with respect to t (but see Section 5).

Thus the model we consider is the following

$$u_t + g(x,u)_x = 0, \quad x \in \mathbb{R},\ t > 0, \qquad u(x,0) = u_0(x), \quad x \in \mathbb{R}. \tag{2.6}$$

By a solution we understand a weak solution in the usual sense, i.e.,

$$\iint_\Pi \big(u\varphi_t + g(x,u)\varphi_x\big)\,dtdx + \int_{\mathbb{R}} u_0(x)\varphi(x,0)\,dx = 0 \tag{2.7}$$

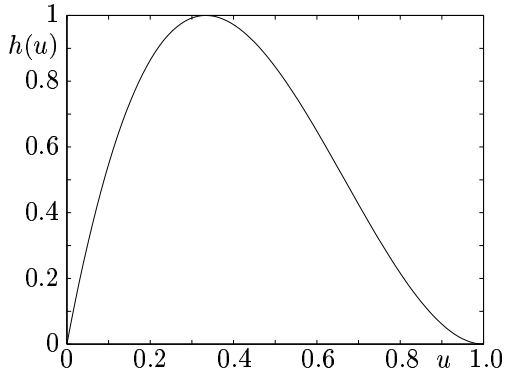

FIGURE 2. The Kynch batch flux density function $h(u) = \frac{27}{4}u(1-u)^2$.

for all test functions $\varphi \in C_0^\infty(\Pi)$, where $\Pi = \mathbb{R} \times [0, \infty)$. The flux function g is defined according to (2.5)

$$g(x,u) = \begin{cases} q_l u & \text{for } x < -1, \\ f\big(q(x), u\big) & \text{for } -1 < x < 1, \\ q_r u + (q_l - q_r)u_{\mathrm{F}} & \text{for } x > 1. \end{cases} \tag{2.8}$$

Recall that $q_l \leq 0 \leq q_r$. The "interior" flux function f is defined as

$$f(q,u) = q\,(u - u_{\mathrm{F}}) + h(u) + q_l u_{\mathrm{F}}. \tag{2.9}$$

For the plots and numerical examples in this paper we have used the function

$$h(u) = \frac{27}{4}\,u(1-u)^2, \tag{2.10}$$

see Figure 2. The mixture flow velocity q has a discontinuity at $x = 0$,

$$q(x) = \begin{cases} q_l & \text{for } x < 0, \\ q_r & \text{for } x > 0. \end{cases}$$

3. Solutions of the Riemann problems

Now we shall solve the Riemann problems at the discontinuities of $g(\cdot, u)$. In this we follow Gimse and Risebro [17]. First we describe the Riemann problems at the overflow and discharge levels $x = \mp 1$, each of which involves one linear and one nonlinear flux function.

For $x = -1$, the left flux function is given by $f_l(u) = q_l u$ and the right flux function given by (2.9) with $q = q_l$. Precisely, we wish to solve the initial value problem (2.6) around $x = -1$ and for small t where

$$u_0(x) = \begin{cases} u_l & \text{for } x < -1, \\ u_r & \text{for } x > -1. \end{cases} \tag{3.1}$$

There are two cases to consider depending on the sign of $f(q_l, u_r)$. Let $\tilde{u}$ be defined by

$$f(q_l, \tilde{u}) = 0 \quad \text{and} \quad \tilde{u} > 0. \tag{3.2}$$

If $f(q_l, u_r) > 0$ or $u_r < \tilde{u}$, then the solution is given by a discontinuity moving to the left with speed q_l, separating u_l and 0, and a discontinuity moving to the right with speed $f(q_l, u_r)/u_r$, separating the values 0 and u_r. If $u_r > \tilde{u}$, let u_{m} be given by $u_{\mathrm{m}} = f(q_l, u_r)/q_l$ (see Figure 3). Then the solution is given by a discontinuity moving to the left with speed q_l, separating u_l and u_{m}, and a discontinuity located at $x = -1$ separating u_{m} and u_r. These two cases are shown in Figure 3.

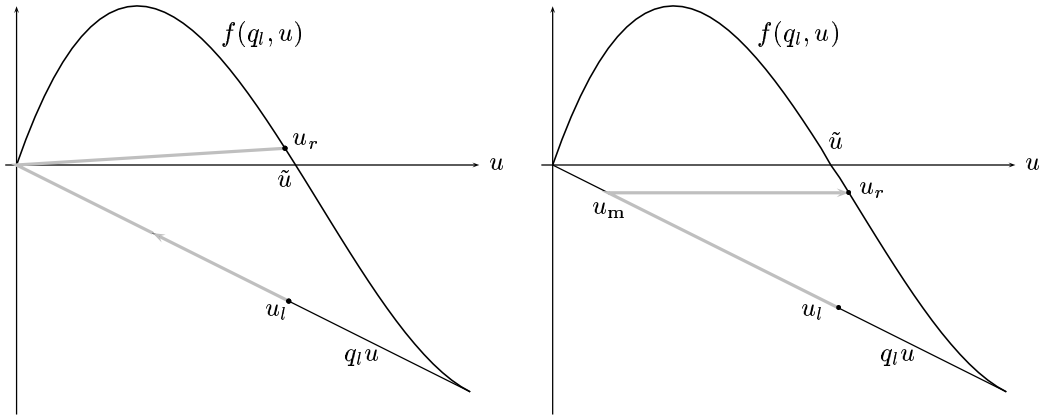

FIGURE 3. Construction of the solution of the Riemann problem (3.1) centered at $x=-1$ with $u_r<\tilde{u}$ (left) and $u_r\geq\tilde{u}$ (right).

For $x=1$ the situation is slightly different since $f(q_r,u)$ can have both a local maximum and a local minimum for u between 0 and 1. Now we wish to solve the Riemann problem defined by the initial datum

$$u_0(x)=\begin{cases}u_l & \text{for } x<1,\\ u_r & \text{for } x>1.\end{cases} \tag{3.3}$$

Let $f_{\min}$ denote the value at the local minimum, and $\bar{u}$ the corresponding u value, i.e.,

$$f(q_r,\bar{u})=f_{\min}, \tag{3.4}$$

and define $\underline{u}$ to be the unique solution of

$$f(q_r,\underline{u})=f_{\min}, \tag{3.5}$$

where $\underline{u}<\bar{u}$. Then the solution of the Riemann problem depends on whether u_l is in the interval $\langle\underline{u},\bar{u}\rangle$ or not. If $u_l\in\langle\underline{u},\bar{u}\rangle$, then the solution is given by a composite u wave from u_l to $\bar{u}$, followed by a q wave with zero speed from $\bar{u}$ to u_{m}, and then by a wave with speed q_r from u_{m} to u_r. Here the term "composite wave" means a wave consisting of a shock followed by a rarefaction. The right middle state u_{m} is given by

$$u_{\mathrm{m}}=\frac{f_{\min}+(q_r-q_l)u_{\mathrm{F}}}{q_r}.$$

If $u_l\notin\langle\underline{u},\bar{u}\rangle$, the solution is similar to the second case at $x=-1$. Now the solution is given by a q wave of zero speed from u_r to u_{m}, followed by a right wave of speed q_r from u_{m} to u_r. Now the middle state u_{m} is given by

$$u_{\mathrm{m}}=\frac{f(q_r,u_l)+(q_r-q_l)u_{\mathrm{F}}}{q_r}.$$

Note that the state immediately to the left $x=1$ is always in the set $[0,\underline{u}]\cup[\bar{u},1]$. See Figure 4 for an illustration. For later use we shall refer to the waves moving out of the interval $[-1,1]$ as *left* and *right* waves respectively. The waves with zero speed sitting at $x=\mp1$ we call left or right *boundary* waves. The waves moving into the region $[-1,1]$ we label u waves.

The Riemann problem defined by the discontinuity in q at $x=0$, which includes the feed mechanism, involves two nonlinear flux functions on either side and is therefore more complicated,

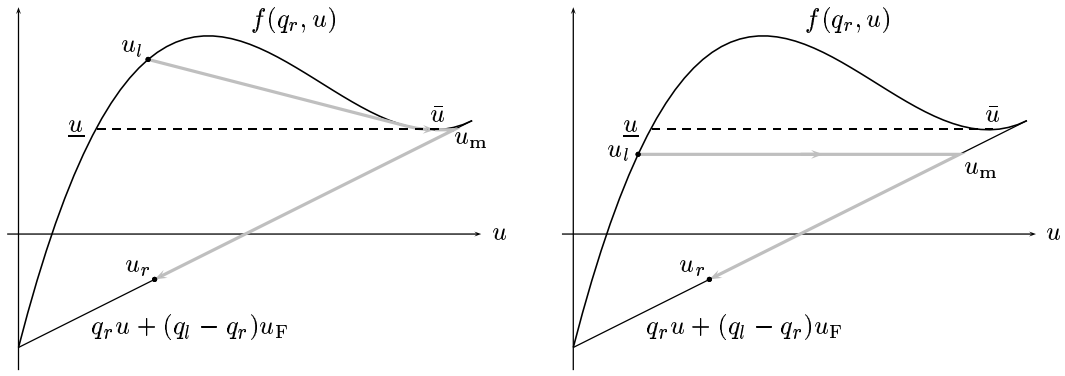

FIGURE 4. Construction of the solution of the Riemann problem (3.3) centered at $x = 1$ with $u_l \in \langle \underline{u}, \bar{u} \rangle$ (left) and $u_l \notin \langle \underline{u}, \bar{u} \rangle$ (right).

but also covered by the general theory in [17]. This Riemann problem is given by

$$u_t + f(q,u)_x = 0, \tag{3.6}$$

$$u(x,0) = \begin{cases} u_l & \text{for } x < 0, \\ u_r & \text{for } x > 0, \end{cases} \qquad q(x) = \begin{cases} q_l & \text{for } x < 0, \\ q_r & \text{for } x > 0, \end{cases} \tag{3.7}$$

where $q_l \le 0 \le q_r$. Here we will demonstrate that there exists a unique entropy solution for all u_l and u_r in $[0,1]$, in the sense that this solution is the limit of a viscous approximation.. This solution consists of u waves, over which q is constant, and a q wave, separating q_l and q_r.

For simplicity, we shall assume that $f(q,u)$ is strictly monotone along the transition curve

$$T := \big\{(u,q) : \partial_u f(q,u) = 0\big\},$$

which is the curve in the (u,q)-plane that joins the local extrema of $f(q,\cdot)$ with respect to u, see Figure 5. This means that the control parameters q_l, q_r and u_{F} are chosen in such a way that

$$\frac{\partial f}{\partial q} \neq 0 \quad \text{on } T, \tag{3.8}$$

which then implies that

$$\text{either } u - u_{\mathrm{F}} < 0 \text{ or } u - u_{\mathrm{F}} > 0 \text{ on } T.$$

We shall assume that the left inequality holds on the left branch of the transition curve, and the right inequality holds on the right branch. Furthermore, we shall assume that q_r is so small that $f(q_r,u)$ has *both* a local maximum and a local minimum in $(0,1)$. We set $\bar{q}$ to be the largest value of q_r for which this is the case. If $h(u)$ is chosen as (2.10) we find that $\bar{q} = 9/4$. Thus in this case we have the the following restrictions on u_{F}:

$$q_r < \frac{9}{4}, \quad \text{and} \quad \frac{2 - \sqrt{1 - 4q_r/9}}{3} < u_{\mathrm{F}} < \frac{2 + \sqrt{1 - 4q_r/9}}{3}. \tag{3.9}$$

We point out that the restrictions (3.9) are not really necessary and are stated for convenience only, since they give fewer cases to discuss when solving the Riemann problem at $x = 0$.

For later use we depict this solution in the (u,q) plane, see Figure 5. We start at a point (u_l, q_l) on the line $q_l \times [0,1]$ and move on a gray path to the point (u_r, q_r). There are two cases to consider depending on the location of u_l. Let $f_{\max}$ be the local maximum of $f(q_r,u)$ (such a maximum exists for $q_r < \bar{q}$), and let $u_1 < u_2$ denote the solutions of

$$f(q_l, u_1) = f(q_l, u_2) = f_{\max}. \tag{3.10}$$

The set of all points (u,q) satisfying $f(q,u) = f_{\max}$ is shown as a dotted curve in Figure 5. Similarly, if $f(q_r,u)$ has a local minimum in u, then we let $f_{\min}$ denote this value, and let u_3 be the unique solution of

$$f(q_l, u_3) = f_{\min}. \tag{3.11}$$

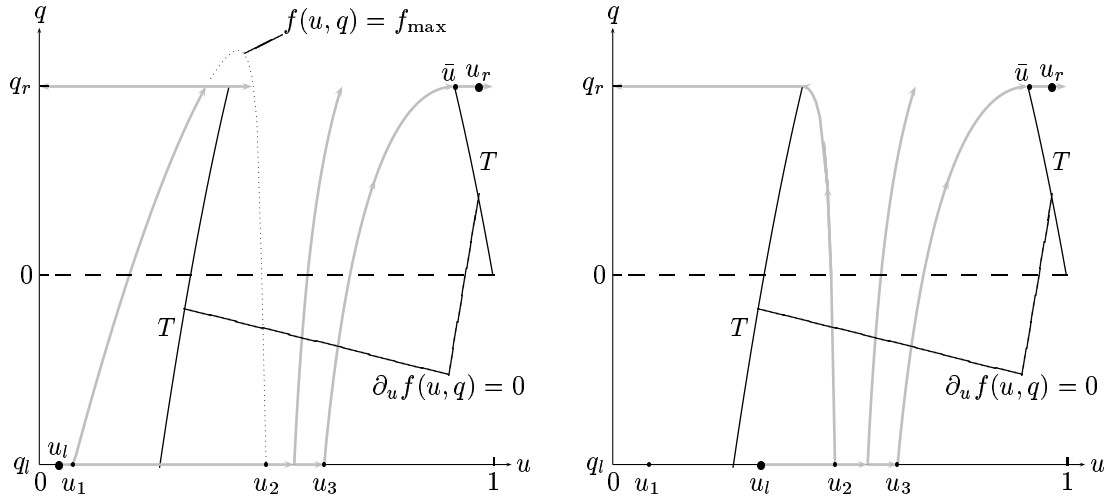

FIGURE 5. Solution of the Riemann problem (3.6) located at $x = 0$ with $u_l < u_1$ (left) and $u_l \geq u_1$ (right).

The solution path is depicted as a gray path in the figures. The horizontal segments are u waves while the segments that move on contour lines of $f(q,u)$ are q waves. To find a particular solution, follow the gray path from (q_l, u_l) (on the lower horizontal line) in the direction of the arrows to the any point (q_r, u_r).

For example, assume that $u_l < u_1$, i.e., we are in the first case, and that u_r lies to the right of the local minimum. Then the solution is given by a u wave connecting u_l and u_3, followed by a q wave connecting (u_3, q_l) with the local minimum, given by the point $\bar{u}$, where $\bar{u}$ is defined by (3.4), where the right branch of T intersects the line $q = q_r$, and finally a u wave connecting the $\bar{u}$ to u_r.

As another example consider the case where u_l is between u_1 and u_2, and u_r is to the left of the local maximum of $f(q_r, u)$. Then, according to the right part of Figure 5, the solution consists of a u wave from u_l to u_2 (this wave will be a shock wave), followed by a q wave connecting (u_l, q_l) with $(\hat{u}, q_r)$, where $\hat{u}$ is the local maximum of $f(q_r, u)$, followed by u wave from $\hat{u}$ to u_r (this wave will be a rarefaction).

Finally, we mention that any Riemann problems occurring inside the intervals $(-1, 0)$ or $(0, 1)$ are Riemann problems for a single scalar conservation law, and are solved by taking the envelope of the flux function, see [20] and Chapter 5 of [6]. Riemann problems outside the interval $[-1, 1]$ are Riemann problems for a linear equation, and their solution is trivial.

4. FRONT TRACKING

4.1. **The front tracking procedure.** Now that we have determined the solutions of all non-standard Riemann problems occurring in our application, we can employ them as a tool for constructing approximations to more general Cauchy problems. The front tracking algorithm we construct closely resembles the ones used in [18, 21, 22]. These algorithms are all based on the fact that for a scalar conservation law of the form

$$u_t + F(u)_x = 0, \quad u(x,0) = u_0(x),$$

one can construct the exact entropy solution if F is piecewise linear on a finite number of intervals, and u_0 takes values in the set of breakpoints of F [19]. We shall make piecewise linear (in u) approximations to $f(q_l, u)$ and $f(q_r, u)$ in such a way that the solution of the Riemann problem at $x = 0$ is easy to compute.

To be specific, choose a (small) positive number δ. Let $\bar{u}_1$ and $\bar{u}_2$ denote the local extrema of $f(q_r, u)$. For $i = 0, \mp 1, \mp 2, \ldots$ let $u_i(q)$ denote the solutions of

$$f\big(q, u_i(q)\big) = f_i, \quad f_i = i\delta. \tag{4.1}$$

In other words, the curves $u_i(q)$ are the contour lines of f in the (u, q)-plane.

With a slight abuse of notation, we define for $q = q_l$ and $q = q_r$ the finite sets of points

$$\{u_i(q_r)\} = \{0, \bar{u}_1, \bar{u}_2, 1\} \cup \{u_i(q_r)\} \cap [0,1], \quad \{u_i(q_l)\} = \{0, u_1, u_2, u_3, 1\} \cup \{u_i(q_l)\} \cap [0,1],$$

where u_1, u_2 and u_3 are defined by (3.10) and (3.11)

$$f(q_l, u_1) = f(q_l, u_2) = f(q_r, \hat{u}) = f_{\max} \quad \text{and} \quad f(q_l, u_3) = f(q_r, \bar{u}) = f_{\min},$$

see also and Figure 5. We order the set $\{u_j(q)\}$ so that $u_{j-1}(q) < u_j(q)$. Then we define a piecewise linear (in u) approximation to $f(q, u)$ by

$$f^\delta(q, u) = f\left(q, u_j(q)\right) + (u - u_j(q)) \frac{f\left(q, u_{j+1}(q)\right) - f\left(q, u_j(q)\right)}{u_{j+1}(q) - u_j(q)} \quad \text{for } u \in [u_j(q), u_{j+1}(q)], \tag{4.2}$$

for $q = q_l$ or q_r. Note that for a fixed (constant) q, the entropy solution of the initial value problem

$$u_t + f^\delta(q, u)_x = 0, \quad u(x, 0) = u_0(x),$$

can be found by front tracking if u_0 is piecewise constant, see [19]. Furthermore, if u_0 takes values in the set $\{u_i\}$, the solution will also take values in this set.

Note also that by construction of f^δ, the solution of the Riemann problems in case f is replaced by f^δ, can still be described by Figure 5 for $x = 0$ and by Figures 4 and 3 for $x = \mp 1$. The breakpoints of f^δ are also chosen such that if for some j the points (q_l, u_j) are connected to (q_r, u) by a q wave, then $u \in \{u_i\}$. This means that if u_j and u_k are breakpoints, the solution of the Riemann problem

$$\begin{cases} u_t + f^\delta\left(q_l, u\right)_x = 0, & u(x,0) = u_j \quad \text{for } x < 0, \\ u_t + f^\delta\left(q_r, u\right)_x = 0, & u(x,0) = u_k \quad \text{for } x > 0 \end{cases}$$

will take values among the breakpoints. Also, since the flux function is linear outside $[-1, 1]$, then a similar observation is valid for Riemann problems defined at $x = \mp 1$. Since f^δ is piecewise linear, the solutions of these Riemann problems will be piecewise constant, and the discontinuities will move with finite speed.

Now we are ready to define the front tracking approximation to (2.6). Let

$$g^\delta(x, u) = \begin{cases} q_l u & \text{for } x < -1, \\ f^\delta(q, u) & \text{for } -1 < x < 1, \\ q_r u + (q_l - q_r) u_{\mathrm{F}} & \text{for } 1 < x, \end{cases} \tag{4.3}$$

and let $u_0^\delta(x)$ be a piecewise constant approximation to u_0 taking values in the set $\{u_i\}$. We define u^δ to be the weak solution to

$$u_t^\delta + g^\delta\left(x, u^\delta\right)_x = 0, \qquad u^\delta(x, 0) = u_0^\delta(x). \tag{4.4}$$

The weak solution u^δ is constructed as follows: First we solve the Riemann problems defined by the discontinuities of u_0^δ and at the points $x = \mp 1$ and $x = 0$. This will give a finite number of discontinuities emanating from the discontinuities of u_0^δ, $x = \mp 1$ and $x = 0$. When these collide, we can solve the Riemann problem defined by the state to the left and right of the collision. This Riemann problem will be of the same type as the initial Riemann problems. Therefore we can continue this process for as many collisions as we like, see [19, 20]. In the next section, we shall see that there will only be a finite number of collisions for all $t > 0$, and hence u^δ can be defined for any t.

4.2. **The Temple functional.** As in [18, 21, 22, 31], it is difficult to show that u^δ has bounded variation, so instead we choose to bound the variation of a nonlinear function of u^δ. Let Ψ be defined as

$$\Psi(q,u) = \int_0^u |\partial_u f(q,\xi)|\, d\xi + f(q,0), \tag{4.5}$$

and set $z = \Psi(q,u)$. In other words, Ψ is a real function of two real variables q and u. Roughly speaking $\Psi(q_1,u_1) - \Psi(q_2,u_2)$ measures "how many" contour lines separate (q_1,u_1) and (q_2,u_2).

The functional Ψ has become known as the Temple functional [31]. Note that Ψ is one-to-one and regular everywhere except on T. We can now view the front tracking solution u^δ as a sequence of waves or *fronts*, left, boundary, u, q or right, going from the left to the right. We label each such front

$$W_l, \quad W_{lb}, \quad W_u, \quad W_q \quad \text{and} \quad W_{rb}$$

respectively. Each of these waves connect a left state (u_1,q_1) to a right state (u_2,q_2). We define the strength of a front according to its type. For a u front W_u we define the strength as

$$F(W_u) = |z(q,u_1) - z(q,u_2)|. \tag{4.6}$$

For a left front W_l we define the strength as

$$F(W_l) = |q_l(u_1 - u_2)|, \tag{4.7}$$

since for a W_l front $q_1 = q_2 = q_l$. Similarly for a right front W_r we define the strength as

$$F(W_r) = |q_r(u_1 - u_2)|. \tag{4.8}$$

For q fronts the definition of the strength is more complicated. Let $u_{\max}$ be the local maximum of $f(q_l,u)$, and set

$$\ell = f(q_l,u_{\max}) - f_{\max}$$

(recall that $f_{\max}$ is the local maximum value of $f(q_r,u)$). For a q wave to the left of the left branch of T, we define its strength as

$$F(W_q) = 4\ell, \tag{4.9}$$

and if the q wave is to the right of the left branch of T, its strength is defined to be

$$F(W_q) = 2\ell. \tag{4.10}$$

It remains to define the strength of the boundary waves. Recall that these are waves of zero speed connecting the interior flux function $f(q,u)$ to the linear flux functions $q_l u$ or $q_r(u - u_{\mathrm{F}}) + q_l u_{\mathrm{F}}$. We start by defining the strength of a left boundary wave. If W_{bl} is a boundary wave connecting u_1 and u_2, then

$$F(W_{bl}) = \begin{cases} 0 & \text{if } u_1 = u_2 = 0, \\ |z(q_l,\tilde{u}) - z(q_l,0)| & \text{otherwise,} \end{cases} \tag{4.11}$$

where $\tilde{u}$ is defined by (3.2), i.e., $f(q_l,\tilde{u}) = 0$ and $\tilde{u} > 0$. In other words, if the solution of the Riemann problem at the left boundary gives a wave moving with positive speed, then the strength of the boundary wave is zero.

We define the strength of the right boundary waves in an analogous manner, though the situation is more complicated since $f(q_r,u)$ can have a local minimum. Then the strength of the boundary wave separating u_1 and u_2 is defined to be

$$F(W_{br}) = \begin{cases} |z(q_r,1) - z(q_r,\underline{u})| & \text{if } u_1 \le \underline{u}, \\ |z(q_r,1) - z(q_r,\bar{u})| & \text{if } u_1 \ge \bar{u}, \end{cases} \tag{4.12}$$

where $\underline{u}$ and $\bar{u}$ are defined by (3.5) and (3.4) respectively. Recall from Section 3 that u_1 cannot be in the interval $(\underline{u},\bar{u})$.

The front tracking construction u^δ can be seen as a sequence of wave paths in the (u,q) plane; $W_1 W_2 \cdots W_N$. For any connected sequence of wave paths, we define F additively

$$F\left(u^\delta\right) = F(W_1 W_2 \cdots W_N) = \sum_i F(W_i). \tag{4.13}$$

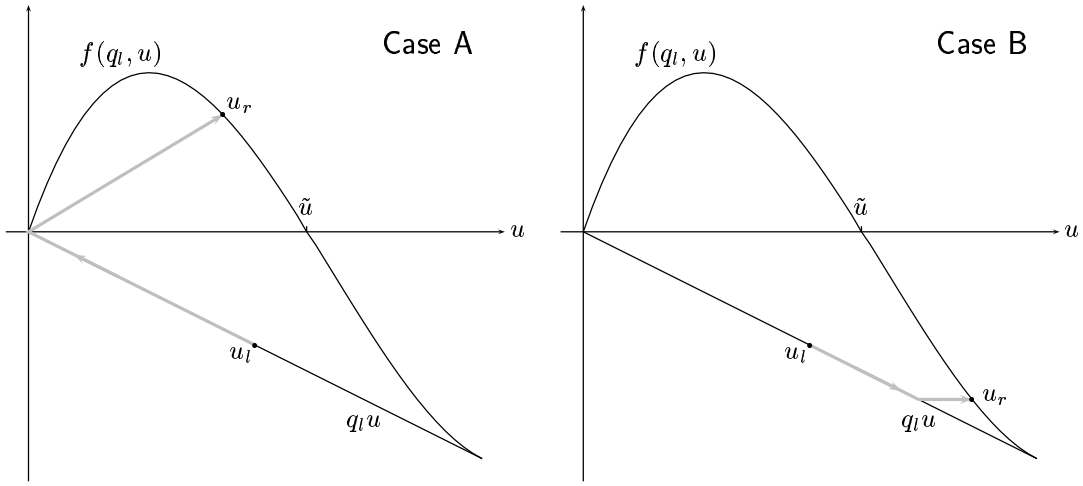

FIGURE 6. The solution of the Riemann problem at $x = -1$. Left: $u_r < \tilde{u}$, right: $u_r \geq \tilde{u}$.

Let $z^\delta = \Psi(q(x), u^\delta)$, then we have that

$$\left|z^\delta\right|_{B.V.} \leq F\left(u^\delta\right).$$

This inequality holds since z^δ is a piecewise constant function in x for each t. Hence $\left|z^\delta\right|_{B.V.}$ is the sum of the absolute value of the jumps in z^δ. For any front W separating z_1 and z_2, we have that

$$|z_1 - z_2| \leq F(W).$$

Furthermore, we have the following crucial lemma:

Lemma 4.1. *Let $w = (q, u)$, and let $[w_l, w_r]$ denote the wave path from w_l to w_r defined by the solution of the Riemann problem with left state w_l and right state w_r. Let γ be any other wave path from w_l to w_r, then*

$$F\left([w_l, w_r]\right) \leq F(\gamma). \tag{4.14}$$

Proof. First we note that if the wave path is a sequence of u waves, then the lemma holds, since the Riemann solution will be the wave path defined by the horizontal line in the (u, q) plane connecting w_l to w_r. This is clearly the "shortest" wave path with respect to F. Next we consider the Riemann problem at the left boundary, $x = -1$. Let $\tilde{u}$ be defined by (4.4). The solution of the Riemann problem depends on whether $u_r < \tilde{u}$ or not. If $u_r < \tilde{u}$ (Case A), then the solution is as indicated in Figure 6. We have that

$$F\left([w_l, w_r]\right) = |q_l u_l| + \left|z(q_l, u_r) - z(q_l, 0)\right|.$$

It is clear that any other path connecting w_l to w_r passing through flux values outside the interval $[q_l u_l, f(q_l, u_r)]$ will have an F value larger than $F[w_l, w_r]$. Furthermore, any path passing through points $f(q_l, u)$ where $u > u_r$ will have a larger F value, since such a path will either pass the same point $f(q_l, u)$ twice, or else involve a boundary wave with zero speed, which will make the F value of the path larger. This shows that in Case A, the path defined by the Riemann solution has the smallest F value.

If $u_r \geq \tilde{u}$ (Case B), then the solution of the Riemann problem is consists of a left wave and a boundary wave, see Figure 6. Now

$$F([w_l, w_r]) = \left|q_l u_l - f(q_l, u_r)\right| + \left|z(q_l, \tilde{u}) - z(q_l, 0)\right|.$$

Also in this case any path involving flux values outside $[q_l u_l, f(q_l, u_r)]$ will have a larger F value than the Riemann solution. Furthermore any path with a single boundary wave inside the region

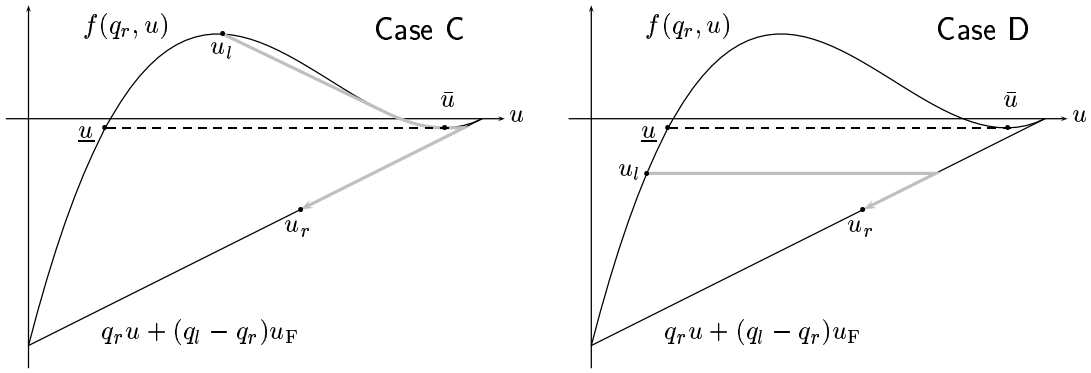

FIGURE 7. The solution of the Riemann problem at $x = 1$. Left: $\underline{u} < u_l < \bar{u}$, right: $u_l \leq \bar{u}$.

$q_l u$ and to the left of $f(q_l, u)$ will have the same F value as that of the Riemann solution. Note that a boundary wave from $u = 1$ to $u = 1$ will not decrease F, since this wave will have strength $|z(q_l, \tilde{u}) - z(q_l, 0)|$. This shows the lemma in this case.

For the Riemann problem at $x = 1$ the situation is similar. Recall that $\bar{u}$ denotes the local minimum of $f(q_r, u)$, and that $\underline{u}$ is defined by $f(q_r, \underline{u}) = f_{\min}$. If $\underline{u} < u_l < \bar{u}$ (Case C), the solution of the Riemann problem is given by a left moving u wave, and a boundary wave followed by a right wave, see Figure 7. In this case

$$F([w_l, w_r]) = |z(q_r, u_l) - z(q_r, \bar{u})| + |z(q_r, \bar{u}) - z(q_r, 1)| = |z(q_r, 1) - z(q_r, u_l)|.$$

If we choose a boundary wave path passing below the line $f = f_{\min}$, the resulting F value will be larger, and also if we choose a path that is not monotone in u before the boundary wave, the F value will be larger. This finishes the proof of the lemma in Case C. If $u_l \leq \underline{u}$ (Case D), the solution of the Riemann problem consists of a boundary wave followed by a right wave, see Figure 7. In this case

$$F([w_l, w_r]) = |z(q_r, 1) - z(q_r, \underline{u})| + |f(q_r, u_l) - q_r(u_r - u_{\mathrm{F}}) + q_l u_{\mathrm{F}}|,$$

where the last term is the strength of the right wave propagating into the region $x > 1$. For another wave path connecting (q_r, u_l) and (q_r, u_r), its F value will be strictly larger if it passes through points in the interval $(\underline{u}, \bar{u})$. Otherwise it will be the same as the F value of the Riemann solution. Hence the lemma holds in Case D. Finally if $u_l \geq \bar{u}$, it is easy to see that the lemma holds.

For the proof of the lemma for a Riemann solution at $x = 0$, the reader should consult Figure 5. First we note that any path that is non-monotone on the horizontal lines q_l and q_r will have an F value greater than that of the Riemann solution. By "non-monotone" we mean that the path must be strictly increasing or decreasing in u for constant q, it can however be increasing on the segment q_l and decreasing on the segment q_r or vice versa. Hence, we need only consider wave paths that have this monotonicity property when proving the lemma in this case. We call such paths u-monotone.

We start by considering $u_l < u_1$, and $u_r < \hat{u}$, where $\hat{u}$ is largest solution of $f(q_r, u) = f(q_l, u_l)$. Then the Riemann solution is given by a q wave separating (u_l, q_l) and (u_{m}, q_r) followed by a u wave separating (u_{m}, q_r) and (u_r, q_r), and

$$F([w_l, w_r]) = 4\ell + |z(q_r, u_{\mathrm{m}}) - z(q_r, u_r)|.$$

Let $\widehat{W}$ denote the q wave to $\hat{u}$. Any u-monotone wave path connecting (u_l, q_l) to (u_r, q_r) with a q wave to the left of or equal to the $\widehat{W}$ will have the same F value as that of the Riemann solution. Wave paths that involve a q wave that is to the right of $\widehat{W}$ will have a larger F value.

Next we assume that $u_r > \hat{u}$. Then any u-monotone wave path, that is also increasing on the segment q_l, will have the same F value as that of the Riemann solution. Any path that is not increasing on the lower horizontal segment will have a larger F value. This proves the lemma if $u_l < u_1$.

Finally, we assume that $u_l \geq u_1$. Then any u-monotone wave path that is monotone on the lower horizontal segment for $u > u_2$, will have the same F value as that of the Riemann solution, whereas any wave path that intersects the the lower segment for some $u \leq u_1$, will have a larger F value, unless $u_l = u_1$, in which case the F value will be that of the Riemann solution. This concludes the proof of the lemma. □

An immediate consequence of this lemma is that

$$F\left(z^\delta(t)\right) \leq F\left(z^\delta(0)\right).$$

In particular the total variation of z^δ is uniformly bounded, independently of δ. Thus we have shown

Lemma 4.2. *Let $u^\delta(x,t)$ denote the front tracking approximation defined in Section 4.1, and let*

$$z^\delta(x,t) = \Psi(q(x), u^\delta(x,t)),$$

where Ψ is the mapping defined in (4.5). Assume that $|\Psi(q(x), u_0(x)|_{B.V.}$ is finite, then

$$\left|z^\delta(\cdot,t)\right|_{B.V.} \leq C,$$

for some constant C independent of δ and t.

Now we shall use Lemma 4.1 to show that the front tracking construction is well defined, in particular that there exists only a finite number of interaction between fronts for $t > 0$. To this end, we shall study some types of collisions closer.

First, if the colliding fronts are both u waves, and the collision results in an increase in the number of fronts, then $F(u^\delta)$ after the collision is strictly smaller than $F(u^\delta)$ before the collision, see, e.g., [19, 20]. We also have that if two fronts collide, and $n > 1$ fronts results from the collision, then F decreases by at least $(n-1)\delta$.

Next we consider collisions of u fronts and the boundary fronts.

We start by studying collisions between the left boundary front and a u front. Note that such a collision always will result in a left front and a boundary front, and possibly a "reflected" u front. Assume that this collision results in three or more fronts. Let the boundary front before the collision separate u_l and u_m, and the u front separate u_m and u_r. We have that $f(q_l, u_m) \leq 0$, and if the collision results in more than two fronts, $f(q_l, u_r) > 0$. Let W_b denote the wave path connecting u_l to u_m followed by the wave path connecting u_m to u_r, and W_a the wave path of the Riemann solution defined by u_l and u_r. Now, W_a must be as the left hand side of Figure 6, since we have a front moving to the right. Furthermore, $f^\delta(q_l, u_r) > 0$, which by construction implies that $f^\delta(q_l, u_r) > \delta$. Therefore

$$\begin{aligned} F(W_b) &= |z(q_l,u_r) - z(q_l,u_m)| + |z(q_l,\tilde{u}) - z(q_l,0)| \\ &= |z(q_l,u_r) - z(q_l,\tilde{u})| + |z(q_l,\tilde{u}) - z(q_l,u_m)| + |z(q_l,\tilde{u}) - z(q_l,u_r)| + |z(q_l,u_r) - z(q_l,0)| \\ &\geq \delta + |z(q_l,\tilde{u}) - z(q_l,u_m)| + \delta + |z(q_l,u_r) - z(q_l,0)| \\ &= 2\delta + F(W_a). \end{aligned} \tag{4.15}$$

Regarding collisions by a u front from the left with the right boundary front, we have that if this collision results in more than two fronts, the middle state u_{m} must be smaller or equal to $\underline{u}$, and the left state greater than $\underline{u}$. In this case an easy calculation shows that (4.15) holds.

Since $F\left(u^\delta(0)\right)$ is finite, and decreases by at least δ each time a front is "reflected" from one of the boundary fronts, since $F \geq 0$, it follows that this can happen at most a finite number of times. Hence after some finite time, t_δ, any front colliding with the boundary fronts will be "transmitted". From these observations, it follows that after a finite time t'_δ, there will be no u fronts with a non-zero speed inside the interval $[-1,1]$, and hence, *for a fixed δ, there will only be a finite number of collisions between fronts in u^δ*. We also have by construction that u^δ is a weak solution to (4.4). We summarize this observation as a lemma.

Lemma 4.3. *Let $u^\delta(x,t)$ be the front tracking construction defined in Section 4.1, and assume that $\left|z^\delta(\cdot,0)\right|_{B.V.}$ is finite. Then $u^\delta(x,t)$ is a weak solution to the initial value problem*

$$u_t^\delta + g^\delta(x,u^\delta)_x = 0, \quad x \in \mathbb{R}, \quad t \in [0,\infty),$$

where g^δ is defined by (4.3). Furthermore, u^δ can be computed using only a finite number of steps.

Proof. We have already shown that u^δ can be computed in a finite number of steps, since to define u^δ we only have to solve a finite number of Riemann problems, and to calculate when and where a finite number of interactions occur. Also, by construction, u^δ is a weak solution. □

Remark. A numerical method that can calculate an approximation for *all* times t in a *finite* number of steps is often called "hyperfast". Therefore, in this terminology, front tracking is a hyperfast method for the initial value problem (1.3).

4.3. **Compactness.** Note that from the definition of z it now follows that

$$\left|g^\delta\left(x,u^\delta(\cdot,t)\right)\right|_{B.V.} \le M,$$

for some finite constant M not depending on δ or t. Let $\alpha_h(t)$ be a smooth approximation to the characteristic function of the interval $[\tau_1,\tau_2]$,

$$\alpha_h(t) = \chi_{[\tau_1,\tau_2]} * \omega_h(t),$$

where ω_h is a standard mollifier with radius h. Then we use the test function $\varphi(x,t) = \phi(x)\alpha_h(t)$ in (2.7), where ϕ is any smooth function with compact support. We let $h \to 0$, and find that

$$\int_{\mathbb{R}} \phi(x)\left(u^\delta\left(x,\tau_2\right) - u^\delta\left(x,\tau_1\right)\right)\,dx + \int_{\tau_1}^{\tau_2}\int_{\mathbb{R}} \phi'(x) g^\delta\left(x,u^\delta(x,t)\right)\,dxdt = 0.$$

From this we find that

$$\begin{aligned}
\left\|u^\delta(\cdot,\tau_2) - u^\delta(\cdot,\tau_1)\right\|_{L^1(\mathbb{R})} &= \sup_{|\phi|\le 1} \int_{\mathbb{R}} \phi(x)\left(u^\delta\left(x,\tau_2\right) - u^\delta\left(x,\tau_1\right)\right)\,dx \\
&\le \int_{\tau_1}^{\tau_2} \left|g^\delta(\cdot,u^\delta)\right|_{B.V.}\,dt \\
&\le M\left(\tau_2 - \tau_1\right). \qquad (4.16)
\end{aligned}$$

Now we have established that u^δ is well defined for any $t > 0$, and satisfies the estimates

$$\left\|z^\delta(\cdot,t)\right\|_{L^\infty(\mathbb{R})} \le M, \quad \forall t > 0, \qquad (4.17)$$

$$\left|z^\delta(\cdot,t)\right|_{B.V.} \le M, \quad \forall t > 0, \qquad (4.18)$$

$$\left\|z^\delta(\cdot,t) - z^\delta(\cdot,s)\right\|_{L^1(\mathbb{R})} \le M(t-s), \quad \forall t,s > 0, t \ge s. \qquad (4.19)$$

for some finite constant M independent of δ and t. To see that the last bound, (4.19), holds, we observe that

$$|z(q,u_1) - z(q,u_2)| = \left|\int_{u_1}^{u_2} |\partial_u f(q,\xi)|\,d\xi\right| \le |u_1 - u_2|\,\|f\|_{\mathrm{Lip}}.$$

From the bounds (4.17), (4.18) and (4.19) it follows from standard theory that the sequence $\left\{z^\delta\right\}$ is strongly compact in L^1_{loc}. Consequently, a subsequence, still labeled $\left\{z^\delta\right\}$, converges a.e. and in L^1_{loc} to some function of bounded variation z. We define

$$u(x,t) = \Psi^{-1}(q(x),z(x,t)). \qquad (4.20)$$

Since $u^\delta = \Psi^{-1}(z^\delta)$ and Ψ^{-1} is continuous, we also have that u^δ converges a.e. and in L^1_{loc} to u, and u is a weak solution to (2.6). The fact that u is a weak solution follows since u^δ is a weak

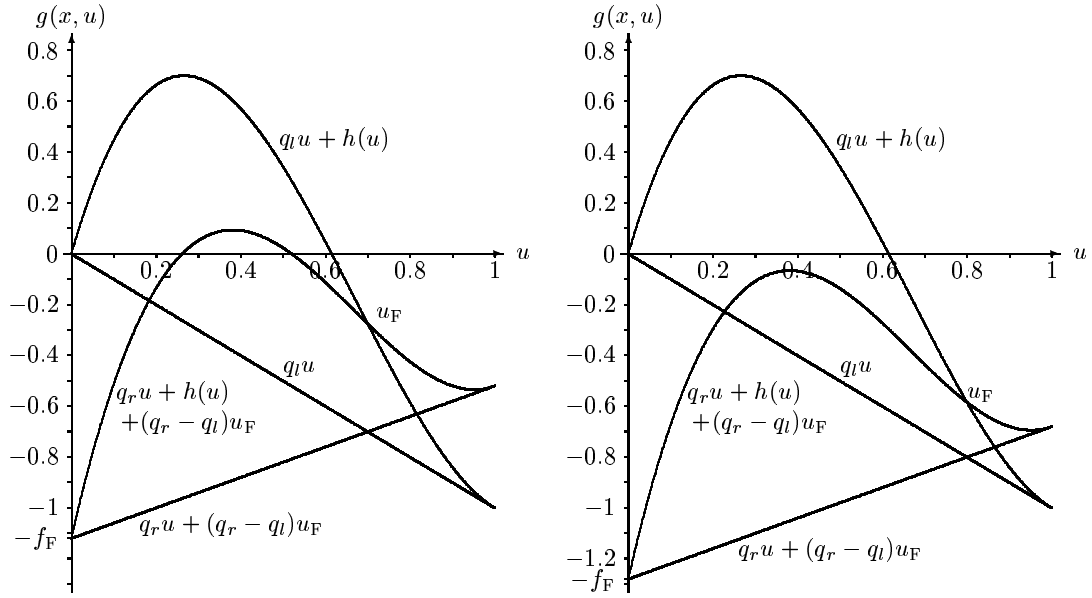

FIGURE 8. The flux density functions for Example 1 (left) and Example 2 (right).

solution of (4.4). For we have that

$$\begin{aligned}
&\iint_{\Pi} u\varphi_t + g(x,u)\varphi_x \, dxdt + \int_{\mathbb{R}} u_0^{\delta}(x)\varphi(x,0)\, dx \\
&\qquad \le \iint_{\Pi} \left|u - u^{\delta}\right| |\varphi_t| \, dxdt + \iint_{\Pi} \left|g(x,u) - g^{\delta}(x,u^{\delta})\right| |\varphi_x| \, dxdt \\
&\qquad\quad + \int_{\mathbb{R}} \left|u(x,0) - u^{\delta}(x,0)\right| |\varphi(x,0)| \, dx + \\
&\qquad \to 0, \quad \text{when } \delta \to 0.
\end{aligned}$$

Hence we have proved the following theorem:

Theorem 4.1. *Assume that the coefficients q_l, q_r and u_{F} satisfy the assumptions* (3.8)*, and that u_0 is such that $|z(u_0)|_{B.V.}$ is finite. Then there exists a weak solution to* (2.6)*, and this weak solution is is a limit of a sequence constructed by front tracking.*

5. NUMERICAL EXAMPLES

Since the front tracking construction is a numerical method, we present here some examples where we have implemented the front tracking method.

5.1. **Constant initial, boundary and control parameters.** In the first two examples, we start from a clarifier-thickener which is initially full of water, i.e., $u_0(x) = 0$ for $x \in \mathbb{R}$. At $t = 0$, we start to fill up the vessel with feed suspension of the concentrations $u_{\mathrm{F}} = 0.7$ in the first and $u_{\mathrm{F}} = 0.8$ in the second case. In both examples we select $q_l = -1$ and $q_r = 0.6$. Figure 8 shows the plots of the four flux density functions involved for each of both examples. These parameters have been chosen in such a way that the structures of the entropy solutions coincide with those of Example 1 and Example 2 by Diehl [15], for which analytical and, in the case corresponding to our choice $u_{\mathrm{F}} = 0.8$, numerical solutions obtained from Godunov's method are presented.

A detailed construction of the entropy solutions is given in [15]. In both cases, the control parameters satisfy

$$u_{\mathrm{F}} Q_{\mathrm{F}} = u_{\mathrm{F}}(q_r - q_l)S = 1.6 u_{\mathrm{F}} S > u_{\max} Q_r \tag{5.1}$$

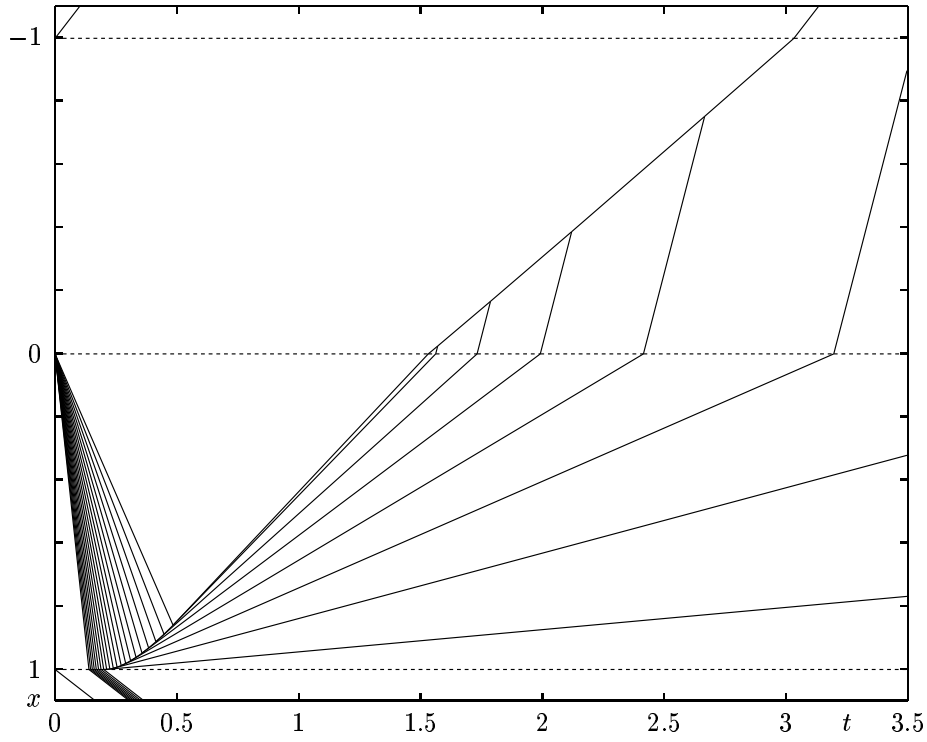

FIGURE 9. Example 1: The fronts in the (t, x)-plane.

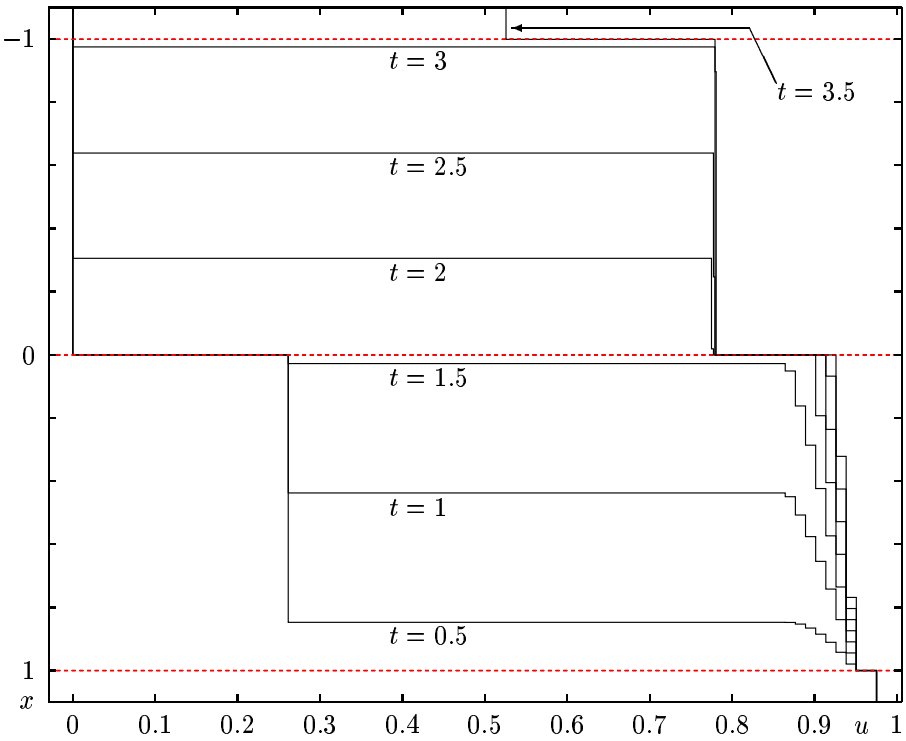

FIGURE 10. Example 1: Concentration profiles at selected times.

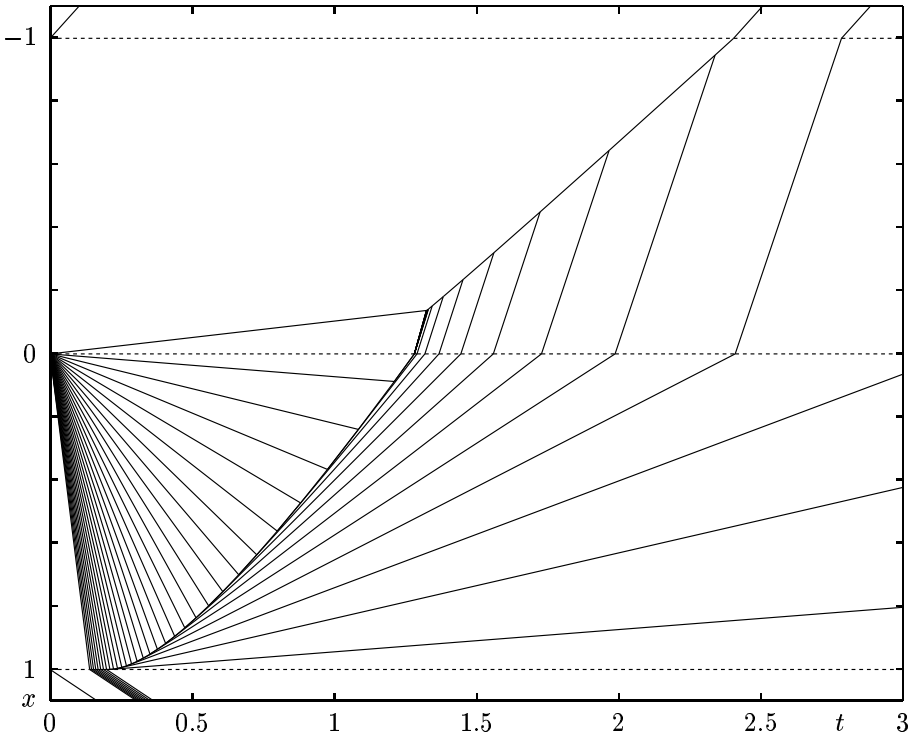

FIGURE 11. Example 2: The fronts in the (t, x)-plane.

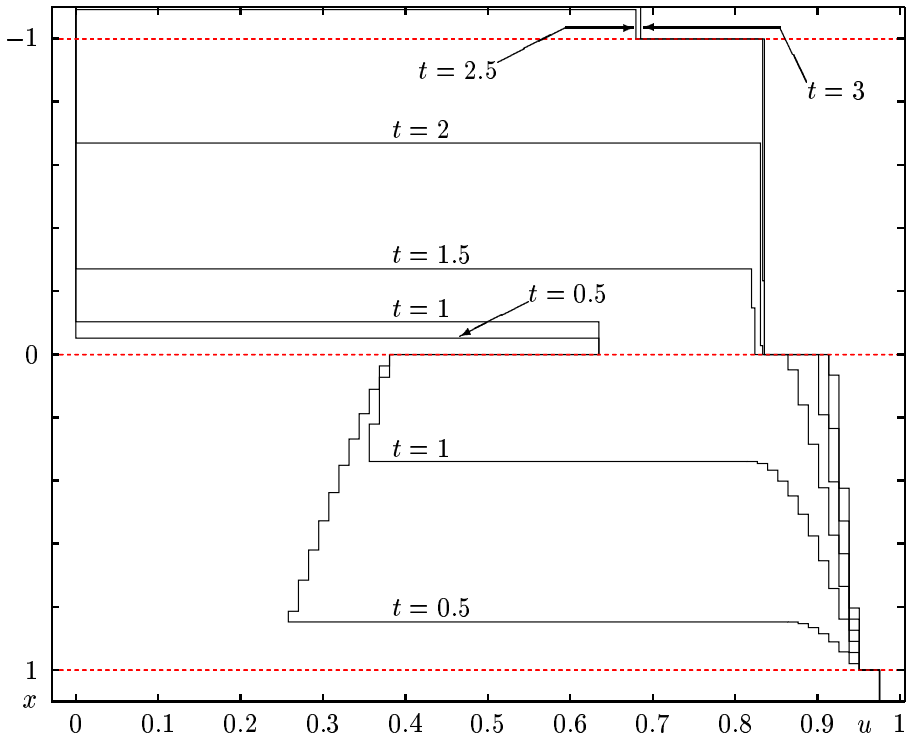

FIGURE 12. Example 2: Concentration profiles at selected times.

time interval	q_l	q_r	u_{F}
[0,0.25)	-0.50	0.40	0.80
[0.25,0.5)	-0.75	0.80	0.40
[0.5,0.75)	-0.50	0.40	0.80
[0.75,1)	-0.75	0.80	0.40
[1,1.25)	-0.50	0.40	0.80
[1.25.1.5)	-0.75	0.80	0.40

TABLE 1. The parameters for Example 3.

which means that the solids feed rate in these example always exceeds the maximum possible solids discharge rate $u_{\max}Q_r \geq u(1,t)Q_r$. Thus the clarifier-thickener is overloaded and one expects that, since the settling zone can not handle the solids feed flux, solids pass into the clarification zone and will eventually leave the unit through the overflow level.

The main qualitative difference between Examples 1 and 2 lies in the behavior at the feed level $x = 0$ for small times. In the first case, with $u_{\mathrm{F}} = 0.7$, this Riemann problem produces a downwards propagating fan, and the concentration in the clarification zone remains initially zero, while for $u_{\mathrm{F}} = 0.8$, the local maximum of $f(q_r, u)$ is negative, and we obtain a centered wave including positive and negative speeds, and the solids will propagate immediately into the clarification zone.

We set the parameter $\delta = 1/80$ in the first two examples. In Figure 9 we show the fronts of Example 1 in the (t,x)-plane, while Figure 10 displays the same result as concentration profiles at selected times. Figures 11 and 12 display the same types of results for Example 2. The numerical results are as expected from the findings of Diehl [15]. Observer that the step-like solution behavior in the thickening zone as seen in Figures 10 and 12 corresponds to regions of continuous transitions of the true entropy solution. Finally, we find confirmed that the solution of Riemann problems at $x = -1$ and $x = 1$ leads to significant changes of the solution values with respect to height: the concentration near the bottom is increased, while the overflow concentration is decreased. This contrasts with the results obtained by using entropy boundary conditions [8].

5.2. **Time dependent coefficients.** It is clear that the analysis of Sections 3 and 4 remains valid if the control parameters q_l, q_r and u_{F} are piecewise constant functions of t. Assuming that $t_0 = 0$ and that the parameters are constant in the time intervals $[t_i, t_{i+1}\rangle$ for $i \geq 0$, we can use front tracking to find a weak solution in each interval $[t_i, t_{i+1}\rangle$, and therefore in $[0,T]$.

To demonstrate this, and to show that front tracking method is able to handle initial data that are not necessarily constant, we show an example where the control parameters are as in Table 1, and the initial data are given by

$$u_0(x) = 0.5 + 0.3\sin\Big(2\pi\max\big(-1,\min(x,1)\big)\Big).$$

For this example, we have used $\delta = 0.005$. In Figure 13 we show the initial data and the final result, and in Figure 14 we show the fronts in the (t,x) plane.

REFERENCES

[1] Barton, N.G., Li, C.-H. and Spencer, S.J., 'Control of a surface of discontinuity in continuous thickeners', *J. Austral. Math. Soc. Ser. B* **33** (1992), 269–289.

[2] Bressan, A., 'Global solutions to systems of conservation laws by wave-front tracking', *J. Math. Anal. Appl.* **170** (1992), 414–432.

[3] Bressan, A., Liu, T.-P. and Yang, T., L^1 stability estimates for $n \times n$ conservation laws. *Arch. Rat. Mech.* **149** (1999), 1–22.

[4] Bürger, R. and Tory, E.M., 'On upper rarefaction waves in batch settling', *Powder Technol.* **108** (2000), 74–87.

[5] Bustos, M.C. and Concha, F., 'Settling velocities of particulate systems: 10. A numerical method for solving Kynch sedimentation processes', *Int. J. Mineral Process.* **57** (1999), 185–203.

[6] Bustos, M.C., Concha, F., Bürger, R. and Tory, E.M., *Sedimentation and Thickening*, Kluwer Academic Publishers, Dordrecht, The Netherlands, 1999.

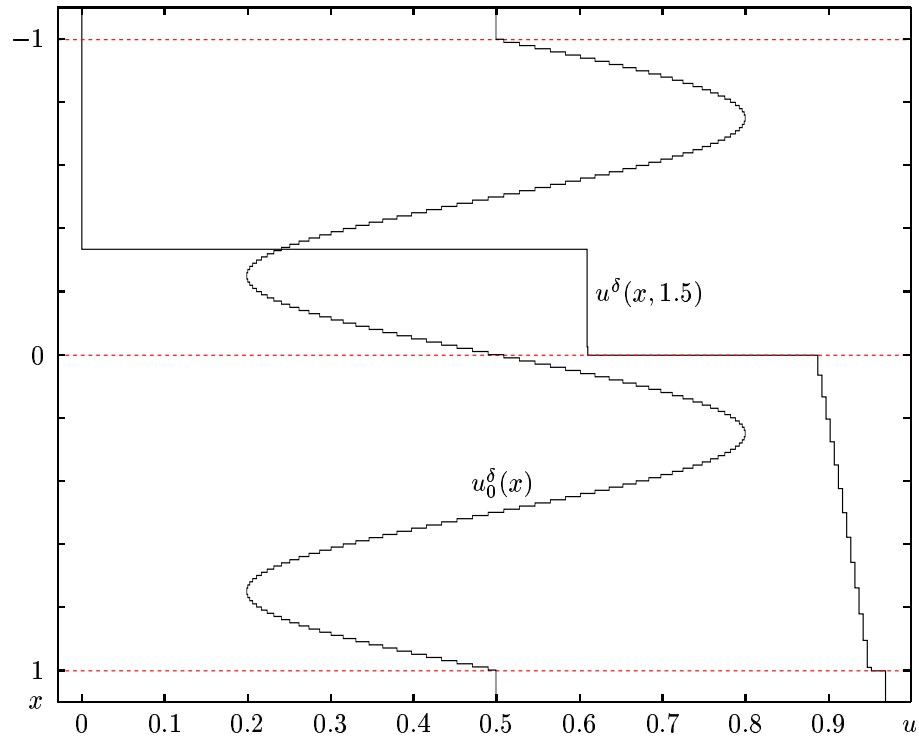

FIGURE 13. Example 3: The initial datum $u_0^\delta(x)$ for the front tracking method and the final concentration profile $u^\delta(x, 1.5)$.

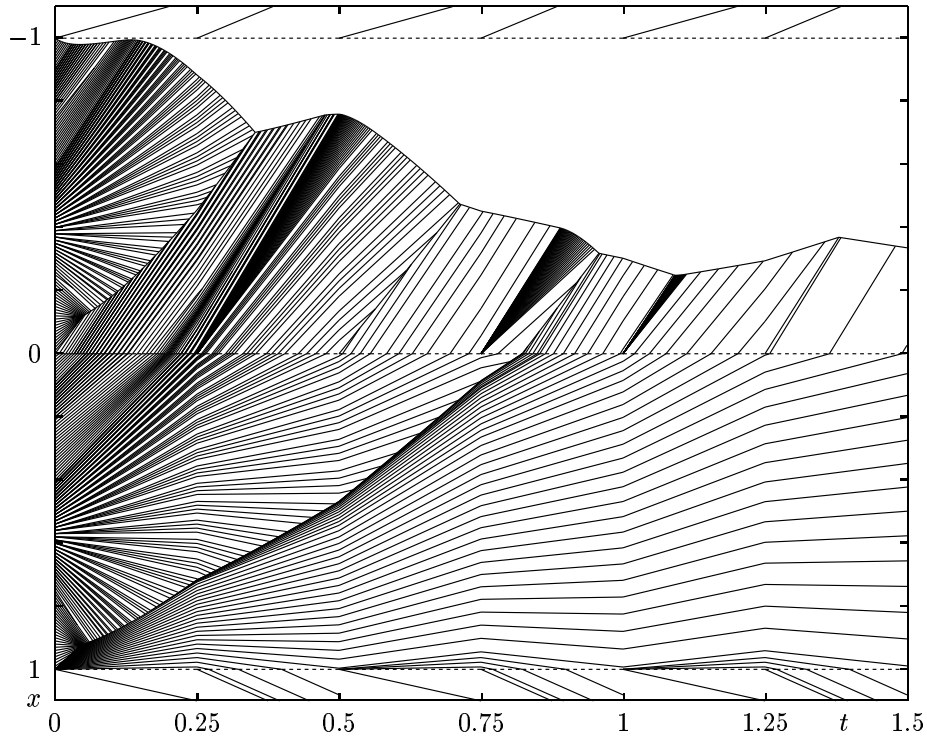

FIGURE 14. The fronts in Example 3.

[7] Bustos, M.C., Concha, F. and Wendland, W.L., 'Global weak solutions to the problem of continuous sedimentation of an ideal suspension', *Math. Meth. Appl. Sci.* **13** (1990), 1–22.
[8] Bustos, M.C., Paiva, F. and Wendland, W.L., 'Entropy boundary conditions in the theory of sedimentation of ideal suspensions', *Math. Meth. Appl. Sci.* **19** (1996), 679–697.
[9] Chancelier, J.P., Cohen de Lara, M. and Pacard, F., 'Analysis of a conservation PDE with discontinuous flux: a model of settler', *SIAM J. Math. Appl.* **54** (1994), 954–995.
[10] Concha, F., Barrientos, A. and Bustos, M.C., 'Phenomenological model of high capacity thickening'. In: Proc. of the *19th International Mineral Processing Congress (XIX IMPC)*, San Francisco 1995, Ch. 14, 75–79.
[11] Dafermos, C.M., 'Polygonal approximations of solutions to the initial value problem for a conservation law', *J. Math. Anal. Appl.* **38** (1972), 33–41.
[12] Diehl, S., 'On scalar conservation laws with point source and discontinuous flux function', *SIAM J. Math. Anal.* **26** (1995), 1425–1451.
[13] Diehl, S.,'A conservation law with point source and discontinuous flux function modelling continuous sedimentation', *SIAM J. Math. Appl.* **56** (1996), 388–419.
[14] Diehl, S., 'Dynamic and steady-state behavior of continuous sedimentation', *SIAM J. Appl. Math.* **57** (1997), 991–1018.
[15] Diehl, S., 'On boundary conditions and solutions for ideal thickener-clarifier units', *Chem. Eng. J.* **80** (2000), 119–133.
[16] DiPerna, R.J., 'Global existence of solutions to nonlinear systems of conservation laws' *J. Diff. Eqn.* **20** (1976), 187-212.
[17] Gimse, T. and Risebro, N.H., 'Riemann problems with a discontinuous flux function'. In: Proc. 3rd Conf. Hyp. Problems, Uppsala, Sweden, 1990.
[18] Gimse, T. and Risebro, N.H., 'Solution of the Cauchy problem for a conservation law with a discontinuous flux function', *SIAM J. Math. Anal.* **23** (1992), 635–648.
[19] Holden, H., Holden, L. and Høegh-Krohn, R., 'A numerical method for first order nonlinear scaler conservation laws in one dimension', *Comp. Math. Appl.* **15** (1988), 595–602.
[20] Holden, H. and Risebro, N.H., *Front Tracking For Conservation Laws*, Springer, to appear.
[21] Klingenberg, C. and Risebro, N.H., 'Convex conservation laws with discontinuous coefficients', *Comm. PDE* **20** (1995), 1959–1990.
[22] Klingenberg, C. and Risebro, N.H., 'Stability of a resonant system of conservation laws modeling polymer flow with gravitation', in preparation.
[23] Kunik, M., 'A numerical method for some initial-value problems of one scalar hyperbolic conservation law', *Math. Meth. Appl. Sci.* **15** (1992), 495–509.
[24] Kunik, M., 'A solution formula for a non-convex scalar hyperbolic conservation law with monotone initial data', *Math. Meth. Appl. Sci.* **16** (1993), 895–902.
[25] Kynch, G.J., 'A theory of sedimentation', *Trans. Faraday Soc.* **48** (1952), 166–176.
[26] Lev, O., Rubin, E. and Sheintuch, M., 'Steady state analysis of a continuous clarifier-thickener system', *AIChE J.* **32** (1986), 1516–1525.
[27] Petty, C.A., 'Continuous sedimentation of a suspension with a nonconvex flux law', *Chem. Eng. Sci.* **30** (1975), 1451–1458.
[28] Risebro, N.H., 'A front-tracking alternative to the random choice method', *Proc. Amer. Math. Soc.* **117** (1993), 1125–1139.
[29] Risebro, N.H. and Tveito, A., 'Front tracking applied to a nonstrictly hyperbolic system of conservation laws', *SIAM J. Sci. Stat. Comput.* **12** (1991), 1401–1419.
[30] Risebro, N.H. and Tveito, A., 'A front tracking method for conservation laws in one dimension', *J. Comp. Phys.* **101** (1992), 130–139.
[31] Temple, B., 'Global solution of the Cauchy problem for a 2×2 non-strictly hyperbolic system of conservation laws', *Adv. Appl. Math.* **3** (1982), 335–375.

(Bürger)
Institute of Mathematics, A
University of Stuttgart
Pfaffenwaldring 57
D-70569 Stuttgart, Germany
E-mail address: buerger@mathematik.uni-stuttgart.de
URL: www.mathematik.uni-stuttgart.de/mathA/lst6/buerger

(Karlsen)
Department of Mathematics
University of Bergen
Johs. Brunsgt. 12
N–5008 Bergen, Norway
E-mail address: kennethk@mi.uib.no
URL: www.mi.uib.no/~kennethk

(Klingenberg)
University of Würzburg
Department of Applied Mathematics and Statistics
Am Hubland
D–97074 Würzburg, Germany
E-mail address: klingen@esprit.iwr.uni-heidelberg.de
URL: ifamus.mathematik.uni-wuerzburg.de/~klingen

(Risebro)
Department of Mathematics
University of Oslo
P.O. Box 1053, Blindern
N–0316 Oslo, Norway
E-mail address: nilshr@math.uio.no
URL: www.math.uio.no/~nilshr